

A MIXED ALGORITHM FOR THE CALCULATION OF RAPIDLY VARYING FLUID FLOWS: THE IMPULSIVELY STARTED CIRCULAR CYLINDER

ANDREA RINALDO* AND ALDO GIORGINI†

School of Civil Engineering, Purdue University, West Lafayette, Indiana 47907, U.S.A.

SUMMARY

A mixed discrete Fourier transform–Finite difference algorithm is developed and used for the calculation of rapidly changing viscous fluid flows past a circular cylinder. The numerical approach has been designed to overcome certain difficulties arising for high Reynolds number simulations. The foremost advantage of the technique lies in its fast calculations of the convolution sums portraying the convective terms of the governing equations. Third-order spatial discretizations and fourth-order time marching are implemented.

New schemes are proposed for the boundary conditions at the solid wall and at large distances. The techniques are tested on a case study with other schemes (summarized by Roache¹) in order to obtain an optimal choice. Definite indications on the stability and accuracy of boundary condition schemes are achieved. Support for the statement of dominant importance of boundary conditions is also given.

A comparison of computational results with experimental data is presented for the case study of the flow past an impulsively started cylinder at Reynolds number 20.

The time development of the symmetrical zone of recirculation, which is formed at an early stage of the flow, has been studied for $300 \leq Re \leq 9500$ by means of the proposed algorithm. Computational results, comparisons with experimental data² and discussion of upper limits of validity of the procedure will be presented in a companion paper.

KEY WORDS Navier–Stokes Discrete Fourier Transform Finite Difference Short Convolutions No-slip Boundary Condition Far Field Condition

INTRODUCTION

The research presented in this paper aims at developing an accurate algorithm for the calculation of unsteady two dimensional viscous flow past an impulsively started circular cylinder.

Some questions still remain, especially for Reynolds number simulations, although several algorithms have been proposed.^{3–28} These questions are related to:

- (a) The high accuracy required close to the solid boundary where the highest gradients of velocity and vorticity occur. An optimal choice of boundary conditions at the wall is crucial for global accuracy.
- (b) The efficiency of far-field boundary conditions, in particular if attention is focussed on time-dependent fields past an impulsively started cylinder. In such a case, in fact, vorticity is

* Ph.D. Graduate. Present Address: Istituto di Idraulica, Università di Padova, via Loredan 20, 35100 Padova, Italy.

† Associate Professor of Hydromechanics.

initially null throughout the integration domain and is gradually convected and diffused from the boundary only after the start.

- (c) The capability of the algorithm to simulate hydrodynamic instabilities, which are experimentally shown in the wake of the body for $Re > 40$ after an early stage of flow development. Imposed odd symmetries of period π (either achieved by simulating the flow in the upper plane only or by expanding the flow fields in odd functions of $\sin n\theta$) would in fact suppress the phenomenon.
- (d) The influence of the grid systems and the time step at increasing Reynolds numbers. In fact such complex phenomena as birth, growth and decay of secondary vortices rapidly develop in early stages of the wake for $Re > 300$. Higher order of accuracy numerical methods are necessary for the study of such composite mechanisms.²⁸

Only three time-dependent simulations (those of Thoman and Szewczyk¹⁴ up to $Re = 300,000$, Patel²⁴ up to $Re = 600$ and Ta Phuoc Loc²⁸ up to $Re = 1000$) have reached high regimes.

The numerical scheme for the solution of the Navier–Stokes equations, and the optimal boundary condition schemes presented in this paper aim at obtaining deeper insight into the nature of initial unsteady flows past the cylinder at high Reynolds number regimes. Hence, all of the above potential problems had to be faced with the additional constraint of tailoring all the tools to the available computational facilities (Purdue University's CDC 7600 computer, with a maximum allowance of CM 200,000 words for special jobs).

A discrete Fourier transform (suitable for fast and accurate computations) of the flow fields permits elimination of forced odd symmetries of the velocity field. Fast algorithms for the evaluation of the convolution sums portraying the non-linearities of the model have been implemented.²⁹

Efficient and conceptually appealing far-field boundary conditions at infinity reduce noticeably the size of the integration domain, thus allowing for finer mesh sizes and higher resolutions. Boundary conditions for the updated value of the wall vorticity (summarized and critically discussed by Roache¹) are tested. Optimal conditions are pointed out: they are remarkably stable and at least third-order accurate.

Tests of accuracy and convergence for the numerical approach have been performed for the flow past an impulsively started cylinder at $Re = 20$. This regime has long been studied, thus yielding an ideal test case for all computed scalar and vectorial fields.

The mechanism of creation of secondary vortices in the early stages of flow past an impulsively started circular cylinder has been analysed by the proposed method for $300 \leq Re \leq 9500$. The results and the comparison with experimental visualizations (yielding the basis for discussion of upper limits of validity for the approach) will be presented in a companion paper.

MATHEMATICAL FORMULATION AND COMPUTATIONAL APPROACH

The particular geometry of the problem suggests the following stipulations:

- (i) The radius R of the cylinder is chosen as length scale.
- (ii) The free stream velocity U_∞ is chosen as velocity scale.
- (iii) The Navier–Stokes equations are cast in polar co-ordinates.

The symbols used in the mathematical formulation are:

- r = polar co-ordinate (radial component)
- θ = polar co-ordinate (angular component)
- U_∞ = velocity scale (velocity of the free stream)
- Ψ = stream-function scalar field
- t = time variable

- $\bar{\nu}$ = kinematic viscosity of the fluid
- $\bar{\rho}$ = density of the fluid
- Re = Reynolds number, defined as $2U_{\infty}R/\bar{\nu}$
- R = length scale (radius of the cylinder)

With this notation the non-dimensional form of the Navier–Stokes equations, when expressed in terms of vorticity, is

$$\zeta = \frac{1}{\rho} \left[\frac{\partial}{\partial \rho} \rho \frac{\partial}{\partial \rho} \psi + \frac{1}{\rho} \frac{\partial^2 \psi}{\partial \theta^2} \right] \tag{1}$$

$$\frac{\partial \zeta}{\partial \tau} - \frac{1}{\rho} \begin{vmatrix} \frac{\partial \psi}{\partial \rho} & \frac{\partial \psi}{\partial \theta} \\ \frac{\partial \zeta}{\partial \rho} & \frac{\partial \zeta}{\partial \theta} \end{vmatrix} - \nu \nabla^2 \zeta = 0 \tag{2}$$

where the physical quantities have been non-dimensionalized by the above scales as follows:

$$\rho = \frac{r}{R}; \quad \psi = \frac{\Psi}{RU_{\infty}}; \quad \tau = \frac{tR}{U_{\infty}}; \quad \nu = \frac{2}{Re} = \frac{\bar{\nu}}{U_{\infty}R}$$

It is expedient to perform two transformations, both for conceptual and numerical reasons. These are:

- (a) The logarithmic mapping of the radial co-ordinate r . This transformation has been often exploited in analogous calculations.^{10,13,15,17,24,27,30} It defines

$$\rho = e^{\xi} \quad \text{or} \quad \xi = \ln \rho \tag{3}$$

- (b) The introduction of perturbation fields (deviation from uniform flow). Formally the symbol ψ is replaced by $\psi + e^{\xi} \sin \theta$, whereas vorticity is unaffected.

The introduction of the above transformations yields the final form of the boundary value problem:

$$e^{2\xi} \frac{\partial \zeta}{\partial \tau} + \frac{\partial \psi}{\partial \theta} \frac{\partial \zeta}{\partial \xi} - \frac{\partial \psi}{\partial \xi} \frac{\partial \zeta}{\partial \theta} + e^{\xi} \left(\cos \theta \frac{\partial \zeta}{\partial \xi} - \sin \theta \frac{\partial \zeta}{\partial \theta} \right) = \nu \left[\frac{\partial^2}{\partial \xi^2} + \frac{\partial^2}{\partial \theta^2} \right] \zeta \tag{4}$$

$$\zeta = -e^{-2\xi} \left[\frac{\partial^2}{\partial \xi^2} + \frac{\partial^2}{\partial \theta^2} \right] \psi \tag{5}$$

On the surface of the body, the no-slip boundary conditions are

$$\psi = \frac{\partial \psi}{\partial \xi} = -\sin \theta \quad \text{for} \quad \xi = 0 \tag{6}$$

and the conditions at infinity become

$$\psi = \frac{\partial \psi}{\partial \xi} = 0 \quad \text{for} \quad \xi = \infty \tag{7}$$

If the stream function $\psi(\xi, \theta, t)$ and vorticity $\zeta(\xi, \theta, t)$ are expanded in Fourier series as

$$\psi(\xi, \theta, t) = \sum_{\kappa=-\infty}^{\infty} \psi_{\kappa}(\xi, t) e^{i\kappa\theta} \tag{8}$$

$$\zeta(\xi, \theta, t) = \sum_{\kappa=-\infty}^{\infty} \zeta_{\kappa}(\xi, t) e^{i\kappa\theta} \tag{9}$$

where $\psi_{-\kappa}(\xi, t) = \psi_{\kappa}^*(\xi, t)$ and $\zeta_{-\kappa}(\xi, t) = \zeta_{\kappa}^*(\xi, t)$, and if (8) and (9) are substituted into both (4) and (5), the following systems of equations are obtained (where, for brevity, $\zeta_{\kappa} = \zeta_{\kappa}(\xi, t)$ and $\psi_{\kappa} = \psi_{\kappa}(\xi, t)$):

$$e^{2\xi} \frac{\partial \zeta_{\kappa}}{\partial t} + \text{Conv} [i\kappa\psi_{\kappa} | \zeta'_{\kappa}] - \text{Conv} [\psi'_{\kappa} | i\kappa\zeta_{\kappa}] + \frac{e^{\xi}}{2} (\text{Conv} [\delta(\kappa^2 - 1) | \zeta'_{\kappa}] + \text{Conv} [i^{\kappa}\delta(\kappa^2 - 1) | i\kappa\zeta_{\kappa}]) \tag{10}$$

$$-v(\zeta''_{\kappa} - \kappa^2\zeta_{\kappa}) = 0, \quad \kappa = -\infty, \dots, \infty$$

$$\psi''_{\kappa} - \kappa^2\psi_{\kappa} = -e^{2\xi}\zeta_{\kappa}, \quad \kappa = -\infty, \dots, \infty \tag{11}$$

where, given any two functions $F_{\kappa}(\xi, t)$ and $G_{\kappa}(\xi, t)$, their convolution is defined as

$$\text{Conv} [F_{\kappa} | G_{\kappa}] = \sum_{\kappa'=-\infty}^{\infty} F_{\kappa'} G_{\kappa-\kappa'} = \sum_{\kappa'=-\infty}^{\infty} F_{\kappa-\kappa'} G_{\kappa'} \tag{12}$$

The simultaneous solution of the coupled systems (10) and (11) with boundary conditions

$$\psi_1(0, t) = \psi'_1(0, t) = \frac{i}{2}$$

$$\psi_{-1}(0, t) = \psi'_{-1}(0, t) = -\frac{i}{2}$$

and

$$\psi_{\kappa}(0, t) = \psi'_{\kappa}(0, t) = 0 \quad \text{for } \kappa^2 \neq 1 \tag{13}$$

is equivalent to the solution of (4) and (5) with boundary conditions (6) and (7).

In the approach just presented the θ dimension has been discretized by Fourier series expansion, but the continuum $0 < \theta < 2\pi$ has been replaced by the discrete infinity $\kappa = 0, \pm 1, \dots, \pm \infty$. The necessary reduction of the range of κ to a finite value could be accomplished by series truncation,^{16,17,24} but, in view of the algorithmic advantages introduced by it, the discrete Fourier transform (DFT) approximation has been used here. According to this approach, a function $f(\xi, \theta, t)$ is replaced by its sample chain $f_j(\xi, t) = f(\xi, j2\pi/N, t), j = 1, \dots, N$, and the Fourier series coefficient $f_{\kappa}(\xi, t)$ is replaced by the discrete Fourier coefficient $\tilde{f}_{\kappa}(\xi, t)$ given by

$$f_j(\xi, t) = \sum_{\kappa=0}^{N-1} \tilde{f}_{\kappa}(\xi, t) (e^{i2\pi})^{(jk/N)} = \sum_{\kappa=0}^{N-1} \tilde{f}_{\kappa}(\xi, t) W_N^{jk} \tag{14}$$

where W_N is the first N th root of 1. If N is sufficiently large, $\tilde{f}_{\kappa}(\xi, t)$ approximates $f_{\kappa}(\xi, t)$ for values of κ not too close to $N/2$.

The algorithmic advantages of the DFT (discrete Fourier transform) formulation with respect to the standard spectral method are constituted by the fact that its operations can be performed by means of the fast Fourier transform (FFT) algorithm,³¹ and that related non-cyclic convolutions can be performed very efficiently by the short convolution (SC) algorithm.²⁹

The approximation changes formally the systems (10) and (11): the symbols ψ and ζ are replaced by $\tilde{\psi}$ and $\tilde{\zeta}$, the range $\kappa = -\infty, \dots, \infty$ is replaced by $\kappa = 0, \dots, N-1$, and the operator $\text{Conv} [|]$ is replaced by

$$\text{NCConv} [\tilde{F}_{\kappa} | \tilde{G}_{\kappa}] = \sum_{\kappa'=0}^{2N-1} \tilde{F}_{\kappa'} \tilde{G}_{\kappa-\kappa'} = \sum_{\kappa'=0}^{2N-1} \tilde{F}_{\kappa-\kappa'} \tilde{G}_{\kappa'} \tag{15}$$

where $\tilde{F}_\kappa = \tilde{F}_\kappa$ for $0 \leq \kappa \leq \frac{N}{2} - 1$, $\tilde{F}_\kappa = \tilde{F}_{\kappa-N}$ for $\frac{3}{2}N + 1 \leq \kappa \leq 2N - 1$ and $\tilde{F}_\kappa = 0$ for $\frac{N}{2} \leq \kappa \leq \frac{3}{2}N$, and analogously for \tilde{G}_κ .

The operator NCCConv (non-cyclic convolution) can be treated as an ordinary convolution sum by appending zeros to the arrays to convolve. The short convolution (SC) algorithm²⁹ has been implemented for the fast calculation of non-cyclic convolutions, allowing also for slight reduction in storage requirements.

The equations to solve numerically are therefore

$$e^{2\xi} \frac{\partial \tilde{\zeta}_\kappa}{\partial t} + \text{NCCConv} [i\kappa \tilde{\psi}_\kappa | \tilde{\zeta}'_\kappa] - \text{NCCConv} [\tilde{\psi}'_\kappa | i\kappa \tilde{\zeta}_\kappa] - \nu(\tilde{\zeta}''_\kappa - \kappa^2 \tilde{\zeta}_\kappa) + R_\kappa = 0, \quad \kappa = 0, \dots, \frac{N}{2} - 1 \tag{16}$$

where

$$R_\kappa = \frac{e^\xi}{2} [\tilde{\zeta}'_{\kappa-1} + \tilde{\zeta}'_{\kappa+1} + (\kappa + 1)\tilde{\zeta}_{\kappa+1} - (\kappa - 1)\tilde{\zeta}_{\kappa-1}] \quad \text{for } \kappa \neq 0$$

$$R_0 = \frac{e^\xi}{2} [\tilde{\zeta}'_{-1} + \tilde{\zeta}'_1 + \tilde{\zeta}_{-1} + \tilde{\zeta}_1] = e^\xi R[\tilde{\zeta}'_1 + \tilde{\zeta}_1]$$

and where $R[\]$ stands for ‘real part of’, and

$$\tilde{\psi}''_\kappa - \kappa^2 \tilde{\psi}_\kappa = -e^{2\xi} \tilde{\zeta}''_\kappa, \quad \kappa = 0, \dots, N/2 - 1 \tag{17}$$

The boundary conditions are formally given by (13) where ψ is replaced by $\tilde{\psi}$.

The spectral reduction of the Navier–Stokes equations to the system (16) and (17) transforms the mathematical problem into a time dependent boundary value problem in the variable ξ which is amenable to a classic computational approach. The solution starts with the establishment of initial conditions for the complex fields $\tilde{\psi}_\kappa, \tilde{\zeta}_\kappa$. The computational cycle begins by implementing some finite difference equation analogue of the partial differential equation for the Fourier coefficients. The values of the time derivatives of vorticity are used to obtain the vorticity field at a new time level. Such updated values allow the solution of (17), with the constraints of far-field and no-slip boundary conditions. The last step in the computational cycle consists of the calculation of new values of $\tilde{\zeta}_\kappa$ on the boundaries of the domain, usually endowed with the greatest spatial variations and affected by non-centred approximations.

Two types of discretizations are therefore needed:

- (a) spatial discretization for the evaluation of the derivatives of $\tilde{\zeta}_\kappa$ and $\tilde{\psi}_\kappa$
- (b) time discretization for time advancement.

As far as step (a) is concerned, if a field $\tilde{\zeta}_\kappa$ is given, the derivatives f'_i and f''_i are estimated by five-point centred finite difference schemes. These are (let $f_i = f(i\Delta\xi) = -e^{-2i\Delta\xi} \tilde{\zeta}_\kappa(i\Delta\xi)$; the index κ has been dropped for ease of notation):

- (i) for the boundary points ($i = 0$):

$$f'_0 = \frac{-25f_0 + 48f_1 - 36f_2 + 48f_3 - 25f_4}{12\Delta\xi} + O(\Delta\xi^4) \tag{18}$$

$$f''_0 = \frac{35f_0 - 104f_1 + 114f_2 - 56f_3 + 11f_4}{12\Delta\xi^2} + O(\Delta\xi^3) \tag{19}$$

(ii) for the points next to the boundary ($i = 1$):

$$f'_1 = \frac{-3f_0 - 10f_1 + 18f_2 - 6f_3 + f_4}{12\Delta\xi} + O(\Delta\xi^4) \quad (20)$$

$$f''_1 = \frac{11f_0 - 20f_1 + 6f_2 + 4f_3 - f_4}{12\Delta\xi^2} + O(\Delta\xi^3) \quad (21)$$

(iii) and for all the other points i :

$$f'_i = \frac{-f_{i-2} + 8f_{i-1} - 8f_{i+1} + f_{i+2}}{12\Delta\xi} + O(\Delta\xi^4) \quad (22)$$

$$f''_i = \frac{-f_{i-2} + 16f_{i-1} - 30f_i + 16f_{i+1} - f_{i+2}}{12\Delta\xi^2} + O(\Delta\xi^3) \quad (23)$$

Some static instabilities are intrinsic to the five-points schemes (20), (24). Their application only at one spatial location ($i = 1$) and results of experimental error analysis reported elsewhere³² justify their use.

It is to be noted that, in the actual simulation, the sensitivity of the results to discretization of the interior field turned out to be much less than to boundary conditions. Thus it is possible that simpler finite difference schemes than (18)–(23) would have sufficed.

A somewhat different procedure has been used to evaluate the first derivative of $\tilde{\psi}_\kappa$. In fact, a truncated Taylor expansion about the i th point for the variable $\tilde{\psi}_\kappa$ yields, upon substitution of the constitutive equation of vorticity (17),

$$\begin{aligned} \left. \frac{\partial \tilde{\psi}}{\partial \xi} \right|_i = & \left[\frac{1}{\kappa^2 \Delta \xi^2} (\tilde{\psi}_{i+1} - \tilde{\psi}_i (1 + \kappa^2 \Delta \xi^2 / 2 + \kappa^4 \Delta \xi^4 / 24)) / \Delta \xi \right. \\ & \left. - f_i \frac{\Delta \xi}{2} \left(1 + \frac{\kappa^2 \Delta \xi^3}{12} \right) - \left. \frac{\partial f}{\partial \xi} \right|_i \frac{\Delta \xi^2}{6} - \left. \frac{\partial^2 f}{\partial \xi^2} \right|_i \frac{\Delta \xi^3}{24} \right] + O(\Delta \xi^4) \end{aligned} \quad (24)$$

Equation (24) is appealing from the computational viewpoint since f_i , $\left. \frac{\partial f}{\partial \xi} \right|_i$, $\left. \frac{\partial^2 f}{\partial \xi^2} \right|_i$ and $\tilde{\psi}_\kappa$ have previously been calculated for all values of i .

As far as time discretization is concerned, error considerations (truncation, round-off and propagation errors) suggest the use of algorithms of an order higher than the first. In fact, the accuracy of the integration procedure for the linear elliptic stream-function equation yields acceptable errors already for $\Delta \xi \simeq 0.1$ for any wave number κ . An approximate stability analysis of von Neumann type, performed by neglecting the convolutive terms in equation (17), yields the stability criterion

$$\Delta t < \mu(\kappa) \Delta \xi^2 Re \quad (25)$$

once the spatial discretizations (22) and (23) are enforced. The function $\mu(k)$ decreases with increasing wave numbers and therefore the wave-number cut-off $N/2$ is the most demanding. The relationship between μ and $N/2$ is

$$\mu(N/2) = \frac{12}{30 + 12(N/2\Delta\xi)^2} \quad (26)$$

Hence for $Re = 20$, and a standard cut-off $N/2 = 16$, an error $O(\Delta t)$ at the maximum stable time step is consistently higher than the error predicted for the solution of (17). A second-order procedure (of the Adam–Bashforth type) yields a stability requirement:

$$\Delta t < 0.18533(\Delta \xi)^2 Re \tag{27}$$

which, in turn yields for the test case an $O(\Delta t)^2 = O(\Delta \xi^4 Re^2)$ error which might be large for high Reynolds numbers. For these reasons a standard fourth-order Runge–Kutta scheme has been implemented.

The order of truncation is $O(\Delta t^4) = O(\Delta \xi^8 Re^4)$, which leads to an accuracy which is deemed satisfactory for the study of rapidly evolving phenomena.

The last part of the computational cycle consists of the evaluation of updated stream-function fields via (17). The procedure relies on implicit finite difference schemes for the discretization of the second derivative of the k th coefficient $\partial^2 \tilde{\psi}_k / \partial \xi^2$ in (17). The scheme chosen is (23). Substitution into (17) yields

$$-\tilde{\psi}_{i-2} + 16\tilde{\psi}_{i-1} + (-30 - 12k^2 \Delta \xi^2)\tilde{\psi}_i + 16\tilde{\psi}_{i+1} - \tilde{\psi}_{i+2} = -12\Delta \xi^2 e^{i\Delta \xi \zeta_i} \tag{28}$$

where $\zeta_i = \zeta_k(i\Delta \xi)$ for homogeneity of notation.

Therefore the solution for $\tilde{\psi}_i, i = 1, \dots, M$ (where M is the total number of stations along the ξ direction) constitutes a complex linear system of equations which can be solved efficiently by standard techniques. The complex matrix of the coefficients is symmetric and banded (the bandwidth is equal to 2) but no use has been made of the potential symmetry of the matrix allowing for imposition of far-field boundary conditions. Since $\tilde{\psi}_1$ and $\partial \tilde{\psi} / \partial \xi|_1$ are given as boundary conditions (arising from non-slip conditions at the solid boundary of the cylinder) and since the values of f_i, f'_i, f''_i are known at each time step, a suitable value of $\tilde{\psi}_2$ can be obtained by high-order Taylor expansion suitably modified by substituting (17) and its derivatives. Hence the value of $\tilde{\psi}_2$ would contain updated values of f_1, f'_1, f''_1 , whereas most authors use calculated values of the stream function to connect vorticity at the wall. The special section on boundary conditions will develop this point further.

A modification of the solution procedure can be introduced if the boundary condition for the vorticity at the solid wall is evaluated in time via a discrete set of values of the stream function close to the boundary (later referred as Thom's³³ Jensen's³⁴ or Briley's³⁵ conditions). In such cases, in fact, the evaluation of $\tilde{\psi}_2$ via Taylor's expansion 'downdates' the values of $\tilde{\psi}$ and often yields fatal instabilities. Following the procedure of Briley³⁵ (and the suggestion of Roache¹), the connection between stability and 'consistency' of the adopted schemes is established for $\partial^2 \tilde{\psi} / \partial \xi^2|_{w+1}$ with the same truncation order of the centred scheme adopted elsewhere. Some additional programming effort is required because one term further from the neighbouring nodes of the usual bandwidth is introduced in the matrix equation. Nevertheless a simple Gaussian modification can remove the added implicitness at the first row.

The system can be solved efficiently if the complex matrix is preprocessed in order to factor the coefficients in a way appropriate to pivotal routines. Efficient solving routines require only the storage of one array whose dimension is $(5, N)$, allowing therefore for only slightly larger storage than any explicit technique of solution. Even though the CP time required on a CDC 7600 for solution is about 20 per cent larger, with $N/2 = 16$, than in the analogous case of other explicit solutions,³² the results computed by implicit techniques turned out to be much more accurate³⁶. The decomposition method chosen has been that of Thomas.

The total drag and pressure coefficients, both at the cylinder's surface, have also been calculated. According to the system of reference chosen and with the usual notation, the time-dependent drag

coefficient is

$$C_D = \frac{D}{\frac{\rho U_\infty^2 R}{2}} = \frac{2}{Re} \int_0^\pi \left(\zeta - \frac{\partial \zeta}{\partial \xi} \right)_{\xi=0} \sin \theta d\theta$$

$$= \frac{4}{Re} \sum_{k=0}^{N/2} \frac{(-1)^{k+1} - 1}{1+k^2} (\zeta_k(0, t) - \zeta'_k(0, t)) \quad (29)$$

D being the total drag on the body.

The values of the steady-state pressure coefficients $P(\theta)$ (here defined as $P(\theta) = (p(0, \theta) - P_\infty)/\frac{1}{2}\rho U_\infty^2$; $p(\xi, \theta)$ is the steady state pressure in the fluid; p_∞ is the uniform pressure at large distances from the cylinder) are

$$P(\theta) = P_s + \frac{2}{Re} \int_\theta^\pi \left(\frac{\partial \zeta}{\partial \xi} \right)_{\xi=0} d\theta \quad (30)$$

where P_s is the front stagnation pressure coefficient, obtainable by direct integration of the Navier–Stokes equations along the front stagnation streamline. The result is

$$P_s = 1 + \frac{2}{Re} \int_0^\infty \left(\frac{\partial \zeta}{\partial \theta} \right)_{\theta=\pi} d\xi \quad (31)$$

The integrals (30) and (31) can be evaluated by numerical techniques of suitable accuracy.

BOUNDARY CONDITIONS

Any known attempt to simulate accurately the flow past a circular cylinder has been shown to be very sensitive to the imposition of boundary conditions. As it has been pointed out in the literature¹ the key factors can be found in:

- (a) the implementation of reasonable conditions at large distances (far-field boundary)
- (b) the implementation of boundary conditions at the surface of the cylinder.

In particular, even though conceptually time marching would suffice for the determination of updated values of wall vorticity, combined effects of high gradients and non-centred approximations require the imposition of boundary conditions for ζ at the solid surface. The importance of such a condition (see reference 1 for a comprehensive review of various methods) is considered dominant.

Far-field boundary conditions

Fornberg²⁷ showed the vital influence of far-field boundary conditions on the accuracy of steady-state calculations. Among other interesting results, Fornberg considers the imposition of the free-stream condition ($\psi = 0$ at $\xi = \xi_\infty$) as unnecessarily restrictive since it has to be imposed at very large distances from the body for accurate results. Similar conditions (such as the imposition of $\partial\psi/\partial\xi = 0$ at $\xi = \xi_0$ obtained by adding extra rows of equal values of the function) have been shown not to improve substantially the goodness of the simulation with noticeably shorter integration field.²⁷

Asymptotic formulae for ψ and ζ have been obtained at large distances from the solid boundary by means of an Oseen type of approach which partially accounts for inertial terms.³⁷ The leading terms for ψ and ζ , which are given as a function of Reynolds number and of the total drag

coefficient, hardly match the spectral reductions (8), (9). Fornberg's²⁷ 'mixed' condition also does not easily suit a spectral reduction.

Although high accuracy can be achieved both by imposing an efficient 'mixed' condition and reaching fairly large outer field distances, a new approach tailored to the flow past an impulsively started body has been used in the present work.³⁸

Since the general solution of (17) is

$$\psi = g(f) + Be^{-k\xi} \tag{32}$$

$g(f)$ being the particular integral, it is to be noted that at large distances from the body the values of $f = -e^{2\xi}\zeta_\kappa$ are negligible. Spatial decay of vorticity is in fact much more rapid than the corresponding decay of the perturbation field of the stream function, and therefore an approximate solution at large distances is $\psi = Be^{-\kappa\xi}$, or the solution of the homogeneous analogue of (17). This yields directly

$$\psi_{M+1} = \psi_M e^{-\kappa\Delta\xi}, \psi_{M+2} = \psi_M e^{-2\kappa\Delta\xi} \tag{33}$$

which constitute a set of conditions less restrictive than the assumptions $\psi_{M+1} = \psi_{M+2} = 0$ or $\psi_{M+1} = \psi_{M+2} = \psi_M$. Substitution in the matrix of the coefficients yields the final form of the linear system of equations to be solved by efficient factorization routines. An interesting feature of this condition is that the integration field can be drastically reduced with an 'exact' boundary value in cases—such as that of the impulsively started cylinder—in which vorticity is initially zero throughout the field. As vorticity (produced at the solid boundary, and then convected and diffused throughout the field) spreads away, the integration field must be enlarged proportionally, but fast diffusion rates due to viscosity confine the region of non-null vorticity within a strip much smaller than the perturbation field. A substantial saving of computer time and storage requirements can therefore be achieved.

Boundary conditions at the surface of the cylinder

The implementation of the no-slip condition for $\tilde{\psi}_\kappa(0)$ and $\tilde{\psi}'_\kappa(0)$ is straightforward; the first row of the arrays is, in fact, set to zero except for the second mode, whose imaginary part is 1/2.

The evaluation of the wall vorticity, instead, is difficult and extremely important because vorticity is produced at the solid boundaries. High gradients and non-centred approximations affect to a great extent both accuracy and stability of such values (mirror-image approaches, in fact, eliminate non-centred approximations with only an illusion of higher order accuracy). Wall vorticity can be formally obtained in several ways, some of which will be briefly outlined below.

Method 1 Vorticity at the wall is directly obtained from the no-slip condition. This method is derived from the idea of Thom, conceived as early as 1928 in its first-order formulation.

The stream function $\tilde{\psi}_\kappa(i\Delta\xi)$ (the \sim sign and the κ index are dropped for convenience ($\tilde{\psi}_\kappa(i\Delta\xi) = \psi_i$); $f_i = -e^{2i\Delta\xi}\zeta_\kappa(i\Delta\xi)$) is expanded in a Taylor series about $i = 0$. Truncation at the first order, substitution of (17) (ψ_0 and $\partial\xi/\partial\xi|_0$ are given as boundary conditions), and rearrangement yield

$$f_0 = \frac{2\left(\psi_1 - \psi_0\left(1 + \frac{\kappa^2\Delta\xi^2}{2}\right)\right)}{\Delta\xi^2} - \frac{2}{\Delta\xi} \frac{\partial\psi}{\partial\xi}\Big|_0 + O(\Delta\xi) \tag{34}$$

which is the first-order accurate evaluation of wall vorticity. It is reported to be a reliable tool, often less error-prone than higher order methods.¹

Method 2. A second-order approximation, directly derivable from (34) with second-order truncation, has been obtained, with some further refinement needed because of the presence of $\partial f/\partial \xi|_0$. Woods³⁹ suggested its evaluation by means of a first-order backward difference: even though the method has given good results, some destabilizing effects have also been reported.¹

The method has been tested in two forms (first derivative as Woods' scheme and as (18)) yielding, respectively,

$$f_0 = \frac{3\left(\psi_1 - \psi_0\left(1 + \kappa^2 \frac{\Delta \xi^2}{2}\right)\right)}{\Delta \xi^2} - \frac{3}{\Delta \xi} \frac{\partial \psi}{\partial \xi} \Big|_0 \left(1 + \kappa^2 \frac{\Delta \xi^2}{6}\right) - \frac{f_1}{2} + O(\Delta \xi^2) \tag{35}$$

and

$$f_0 = \frac{72\left(\psi_1 - \psi_0\left(1 + \kappa^2 \frac{\Delta \xi^2}{2}\right)\right)}{112 \Delta \xi^2} - \frac{72}{112 \Delta \xi} \frac{\partial \psi}{\partial \xi} \Big|_0 \left(1 + \frac{\kappa^2 \Delta \xi^2}{6}\right) - \frac{48f_1 - 36f_2 + 48f_3 - 25f_4}{112} + O(\Delta \xi^2) \tag{36}$$

Method 3. Another term of Taylor expansion (34) can be included. Some further refinement problems become manifest because of the introduction of the term involving $\partial^2 f/\partial \xi^2|_0$. Instead of assuming other available approximations^{34,35} (reported in Reference 1), for consistency the second derivative of vorticity at the wall has been evaluated via (19). The result is

$$f_0 = \frac{1}{\left(\frac{25}{96} + \kappa^2 \frac{\Delta \xi^2}{24}\right)} \left[\frac{\left(\psi_1 - \psi_0\left(1 + \kappa^2 \frac{\Delta \xi^2}{2} + \kappa^4\right)\right) \frac{\Delta \xi^4}{24}}{\Delta \xi^2} - \frac{1}{\Delta \xi} \frac{\partial \psi}{\partial \xi} \Big|_0 \left(1 + \kappa^2 \frac{\Delta \xi^2}{6}\right) - \frac{1}{288} (88f_1 - 30f_2 + 136f_3 - 89f_4) \right] + O(\Delta \xi^3) \tag{37}$$

Method 4. This method is a modification of Briley's approach (as in Reference 1). From the presentation of methods 1-3 one can infer that the main drawback of such approaches lies in the need of evaluating $\partial f/\partial \xi|_0$ and $\partial^2 f/\partial \xi^2|_0$ at the boundary for orders of truncation higher than $O(\Delta \xi)$. Non-centred schemes seem to yield static instabilities which may cause solution instability. A consistent approach for eliminating such influences in the calculation of f_0 consists of the following procedure. The Taylor expansions for ψ in terms of $\Delta \xi, 2\Delta \xi, 3\Delta \xi$, are taken and (17) is substituted. 'Consistency' according to Briley requires that the order of truncation for the value of f_0 be the same in the evaluation of $\partial \psi/\partial \xi$ and $\partial^2 \psi/\partial \xi^2$ at $w + 1$. A third-order approximation which is not affected by skewed evaluations of $\partial^2 f/\partial \xi^2, \partial f/\partial \xi$ must be a linear combination $\alpha \psi_1 + \beta \psi_2 + \gamma \psi_3$ such that

$$\begin{aligned} \frac{\alpha}{6} + \frac{4}{3}\beta + \frac{9}{2}\gamma &= 0 \\ \frac{\alpha}{24} + \frac{2}{3}\beta + \frac{27}{8}\gamma &= 0 \end{aligned} \tag{38}$$

which yields, after substitution and some algebra,

$$f_0 = \frac{-85\psi_0 + 108\psi_1 - 27\psi_2 + 4\psi_3}{18\Delta\xi^2} - k^2\psi_0 - \frac{66\psi'_0}{18\Delta\xi} + O(\Delta\xi^3) \tag{39}$$

Equation (39) is a rewriting of equation (3-443) of Roache's book,¹ quoting Briley's work where the differences are due to the different boundary conditions. Following Roache,¹ a 'consistent' modification of the finite difference approximation for ψ at $w + 1$ has been implemented, as described in the computational approach.

Method 5. Vorticity at the wall is obtained from an integral relationship. An analogous approach has been reported by Dennis and Chang,¹⁷ and it has been suited to the present needs by modifications due to the difference in boundary conditions.

From (17), with the usual notation, we can write

$$\tilde{\psi}''_{\kappa} - \kappa^2\tilde{\psi}_{\kappa} = f_{\kappa} \tag{40}$$

with

$$\begin{aligned} \tilde{\psi}_{\kappa}(0) = \tilde{\psi}'_{\kappa}(0) &= \frac{i}{2}, \quad \text{for } \kappa = 1 \\ \tilde{\psi}_{\kappa}(0) = \tilde{\psi}'_{\kappa}(0) &= 0, \quad \text{for } \kappa \neq 1 \end{aligned}$$

If the inner product of (40) with respect to $\langle |e^{-\kappa\xi} \rangle$ is taken, integration by parts yields

$$\int_0^{\infty} f_{\kappa} e^{-\kappa\xi} d\xi = -\tilde{\psi}'_{\kappa}(0) - \kappa\tilde{\psi}_{\kappa}(0) \tag{41}$$

Equation (41) is an integral relationship involving all the values of the vorticity from the wall to the far boundary. When the left side of (41) is calculated by means of any numerical quadrature formula over the grid lines of constant ξ , it gives a formula for f_0 in terms of all the other grid values of $f_{\kappa}(\xi)$ for $\xi \neq 0$. One of the features of the method is that wall vorticity can be calculated by integration right throughout the field rather than from a few isolated values of $\tilde{\psi}$ near $\xi = 0$. High-order integration schemes can be used for accurate evaluations of f_0 . In particular, if fourth-order Cotes' formulae are used, we obtain

$$f_0 = -\frac{45}{2\Delta\xi}(\tilde{\psi}'_{\kappa}(0) + k\tilde{\psi}_{\kappa}(0)) - \frac{1}{7} \sum_{i=1}^{N/4} (7f_j c_i + 32f_{j+1} + 12f_{j+2} + 32f_{j+3} + 7f_{j+4}) \tag{42}$$

where $j = 4i - 3$, $c_i = 1$, if $i \neq 1$, $c_i = 0$ if $i = 1$.

Several other methods have been tested, in order to investigate suitable corrections to both values of f_i at the wall and at the near point, also affected by non-central difference schemes. As an example, a 'mixed' geometrical and integral method can be obtained if equations (34) and (42) are solved for f_0, f_1 . The results have been presented in a previous report.³⁶ Geometrical approximations yielding the boundary value f_0 have been tested in order to smooth out possible errors (due to non-centred approximations for ζ at $w + 1$) by means of curve fitting by least squares. Since (16) can be solved at the solid boundary (with imposition of no-slip conditions), the joint imposition of (17) yields a system of equations involving $\zeta_{\kappa}(0), \zeta''_{\kappa}(0), \tilde{\psi}_{\kappa}(0)$ at each time step. Both equations can be used to update the boundary condition for vorticity, provided that satisfactory hypotheses are made in order to represent the key values $\zeta''(0, k)$ and $\tilde{\psi}''(0, k)$. As an example, parabolic approximations have been tested and discussed in a previous report.^{32, 46}

RESULTS AND DISCUSSION

The flow fields induced by an impulsively started circular cylinder at $Re = 20$ have been calculated.

The numerical experiment aims at a twofold objective: to test the ability of the algorithm to reach

a steady state and to check the accuracy of the solution by comparison with analogous experimental or numerical results.^{7,20,40}

In particular several tests have been imposed on:

- (a) the influence of the radial step of integration $\Delta\xi$, and the time step Δt related by stability criteria
- (b) the influence of the boundary conditions for $\zeta_\kappa(0, t)$.

The comparison with experimental and numerical results has been performed on:

- (i) geometrical parameters: time evolution of the main features of the bubble wake (including length, width and angle of separation)
- (ii) kinematic and dynamic features: time evolution of contour lines of vorticity and stream function; time evolution of wall vorticity; time evolution of total drag; relative pressure distribution at the solid boundary.

For all these quantities extensive experimental or numerical results have been reported in the literature. The basic reference for geometrical parameters has been the paper of Coutanceau and Bouard,⁴¹ in which a detailed experimental visualization of flow patterns evolution has been presented. Several numerical results are available for the flow at $Re = 20$: the time-dependent studies of Kawaguti and Jain⁷ and Collins and Dennis²⁰ are used for comparison. Steady-state parameters have been obtained by Takami and Keller,¹⁵ Nieuwstadt and Keller,¹⁹ Dennis and Chang,¹⁷ Ta²³ and Fornberg.²⁷

The number of modes chosen for the simulation has been $2^5 = 32$ (the related cut-off is $N/2 +$

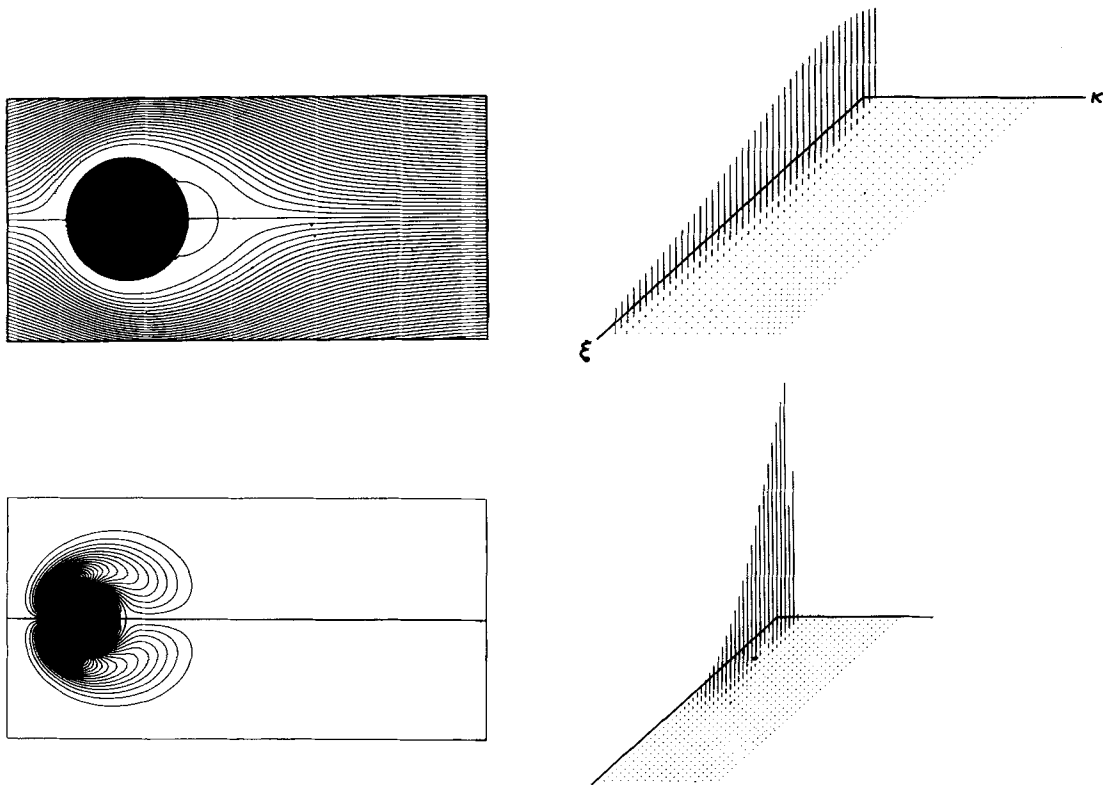


Figure 1. Stream function and vorticity fields with spectral representation at $t = 1.0$ ($Re = 20$)

1 = 17). The size of the integration domain has progressively been enlarged according to the properties of the new far field condition for $\tilde{\psi}_\kappa(\xi_\infty)$ until a maximum radial length $\xi_\infty = 2\pi$ (which corresponds to a radius $r = 565 R$) has been reached. The overall CP time per time step on the CDC 7600 of Purdue University is 20 s with 17 modes and 32 s with 33 modes.

The main results of the calculations for $\Delta\xi = \pi/64$ and for the 'optimal' boundary conditions are shown in Figures 1–3. Time evolution of streamlines, of stream-function spectral representation, of contour lines of vorticity ζ and of related spectral representations are illustrated in Figures 1–3 for $t = 1, 1.5$ and 7.25 . The spectral representations (Figures 1–3) are particularly useful in ascertaining the effectiveness of the wave-number cut-off. An insufficient number of modes would in fact result in the damping up of energy at the high mode boundary which could easily be detectable on the graphic display.

Figure 4 illustrates the convergence properties of the calculated fields for three different values of $\Delta\xi$. The parameter chosen to portray convergence is the integral Ω of vorticity at the solid wall*. Wall vorticity is in fact traditionally considered one of the slowest parameters to converge, and generally the most sensitive.

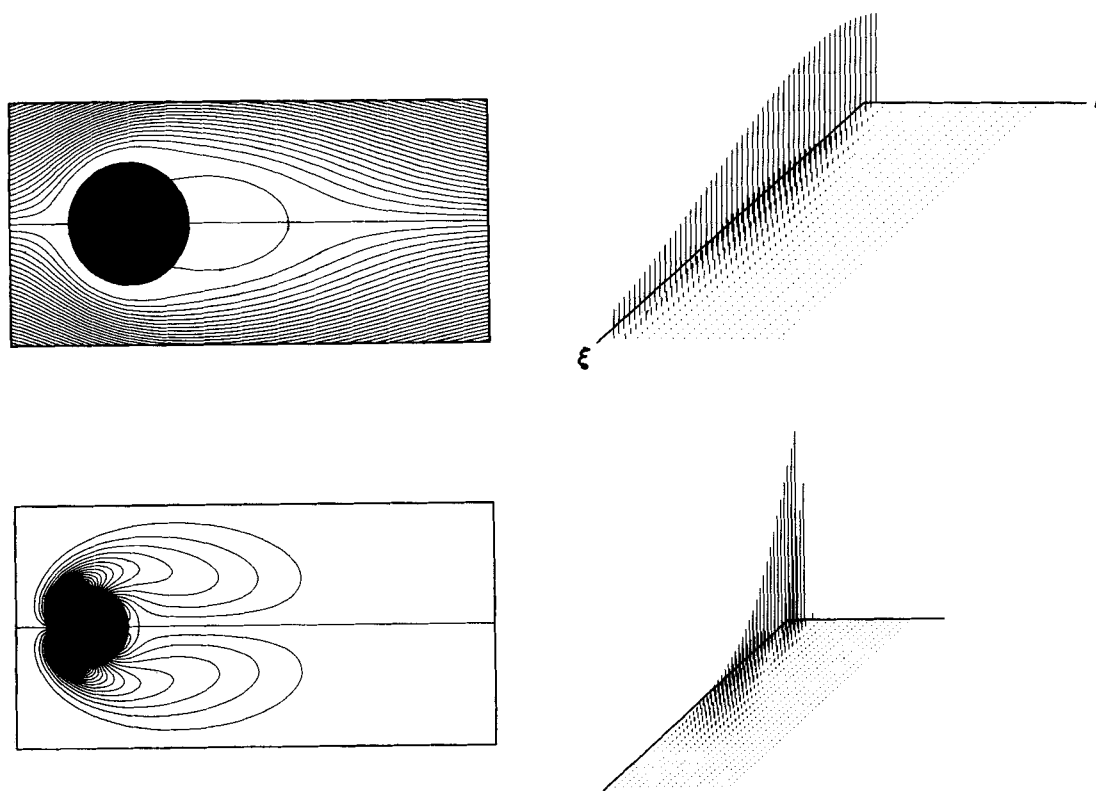


Figure 2. Stream function and vorticity fields with spectral representation at $t = 1.5$ ($Re = 20$)

* This parameter is defined as

$$\Omega = \sum_{-N/2}^{N/2} \left| \zeta^{t+\Delta t}(0, k) - \zeta^t(0, k) \right| = \sum_{-N/2}^{N/2} \left| \zeta_\kappa(0, t + \Delta t) - \zeta_\kappa(0, t) \right|$$

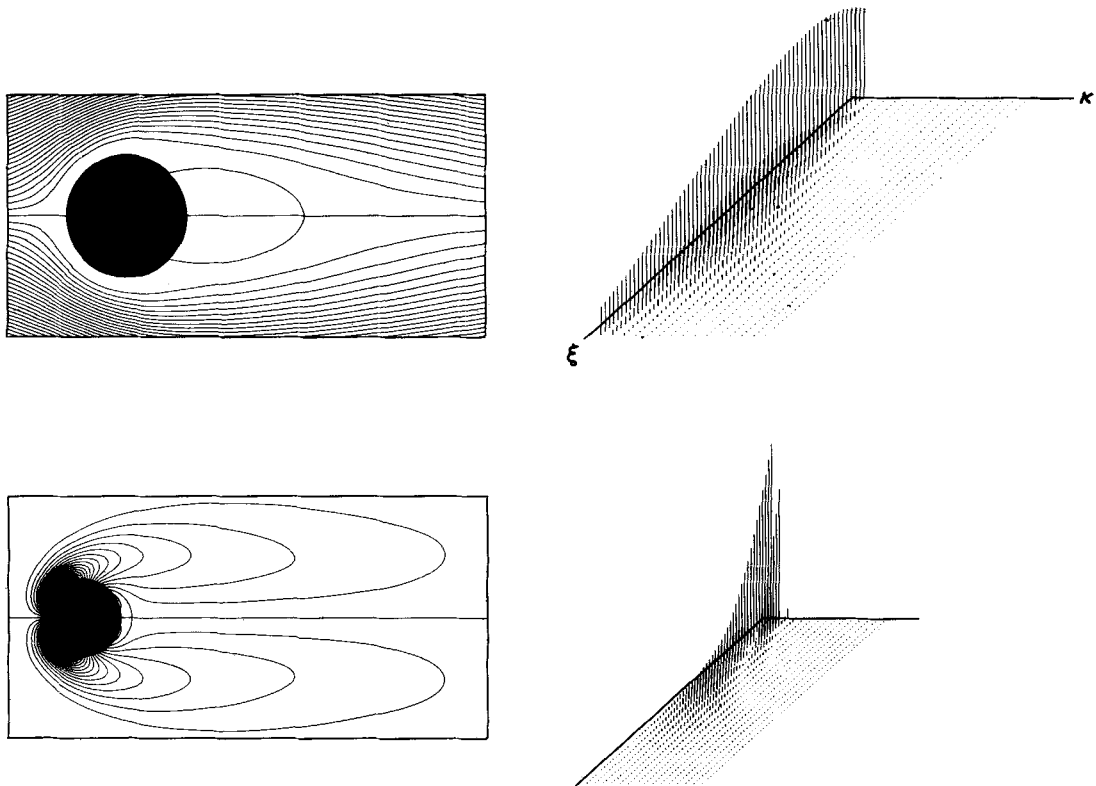


Figure 3. Stream function and vorticity fields with spectral representation at $t = 7.25$ ($Re = 20$)

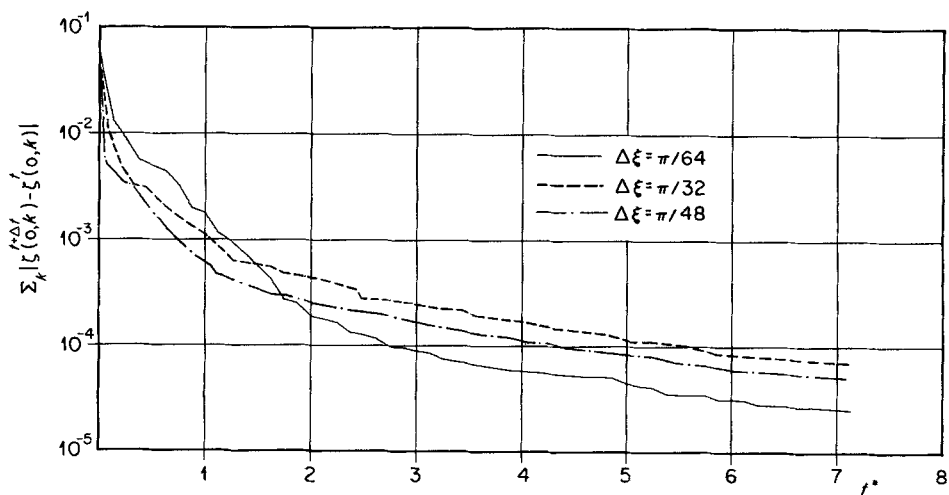


Figure 4. Time evolution of the test of convergence for the study case $Re = 20$

From the results of Figure 4 we can infer that even though convergence to steady state (for which Ω would be identically zero) has not yet been reached, the ability of the algorithm to reach a steady solution at some larger times seems certain. Furthermore, convergence is reached at earlier times for most parameters when $\Omega \cong 10^{-3}$.

Time evolution of the close-wake geometrical parameters

Figure 5 illustrates the evolution of the non-dimensional closed-wake length L/D at $Re = 20$. A coarse radial mesh size ($\Delta\xi = \pi/24$) has been chosen at first, in order to test the effect of different boundary conditions for the wall vorticity. The first-order boundary condition (method 1) yields a convergent and fairly inaccurate solution, the steady length of the wake being 25 per cent larger than the average experimental and numerical results. The second-order approximations of methods 2, 3 turned out to be extremely unstable in any configurations and had to be dropped for $t < 0.2$. It is interesting to point out that method 4, which consists of the third-order approximation for such a boundary condition ('consistent' according to Briley and Roache's definition), yields much more accurate lengths of the wake for the early stages of its development. Unfortunately at $t = 3$ the bubble wake collapses (a phenomenon similar to an aspect ratio effect), yielding a fatal instability of the solution. The implementation of method 4 has been tried also for $\Delta\xi = \pi/64$ with analogous results (Figure 5). Since this method has some analogies with Woods' three-point method (as in Reference 1), it seems plausible that the same unstable behaviour should have been detected by the investigators who made use of it (for instance Panniker and Lavan²²). No mention of 'late' instabilities is made in such papers, although some calculations, interrupted at seemingly arbitrary times, suggest that similar problems might have surfaced later. Best results have been obtained by implementing method 5. The integral relationship weighting all values of vorticity to obtain the boundary value is stable and at least third-order accurate (as the early stage of the length seems to infer). Such a boundary condition is also appealing from the physical viewpoint, since vorticity is created instantaneously at the start of the motion: the integral property respects this fact, making use of the boundary conditions even when vorticity within the outer field is everywhere null. Any other method (either implementing geometrically consistent corrections, or corrections on both points affected by non-centred FD schemes) turned out to be very unstable and had to be dropped before $t = 0.5$.

Method 5 has therefore been chosen for all other calculations. The overall accuracy of the procedure has been tested via a sequence of simulations with reduced mesh sizes $\Delta\xi$. The values chosen are $\Delta\xi = \pi/32, \pi/48, \pi/64$, and the corresponding Δt have been calculated via the approximate stability relationship. The results of the calculations are shown in Figure 5, where the solid line portrays Coutanceau and Bouard's⁴¹ extrapolation for the aspect ratio $\lambda = 0$. Kawaguti and Jain's time dependent results⁷ have also been reproduced. Discrepancies with experiments at larger $\Delta\xi$ can be explained by the strong dependence of the wall vorticity on the radial step $\Delta\xi$. It seems, in fact, that overestimated values of vorticity at the rear of the body greatly affect the length of the bubble wake. It is interesting to observe that different procedures, as far as truncation order and numerical schemes are concerned, yield approximately the same results only because the radial step $\Delta\xi$ chosen has been roughly the same. Further support is obtained by Collins and Dennis³⁰ once their calculations (achieved by a Crank-Nicholson implicit scheme far more sophisticated than Kawaguti and Jain's second-order scheme) have been compared with those of Kawaguti and Jain⁷ at $Re = 40$: with the same radial step $\Delta\xi$, a close evolution of the length is obtained. Roache's¹ statement about fluid dynamic simulations being dominated by boundary conditions is to the point: the accuracy of numerical results seems to depend more strongly on accurate imposition of boundary conditions than on refinements of inner field discretization schemes.

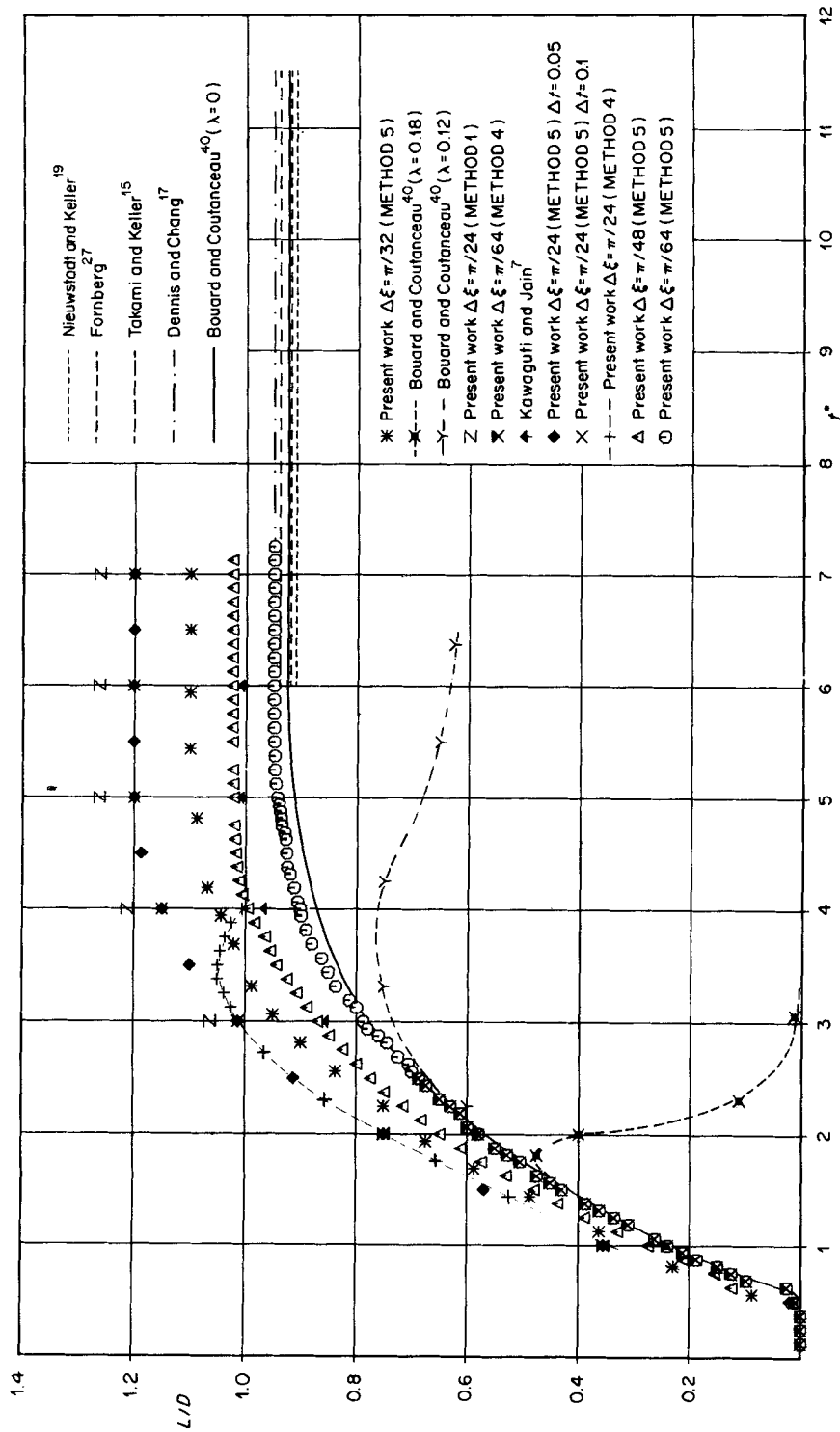


Figure 5. Time evolution of the non-dimensional length of the bubble wake for $Re = 20$

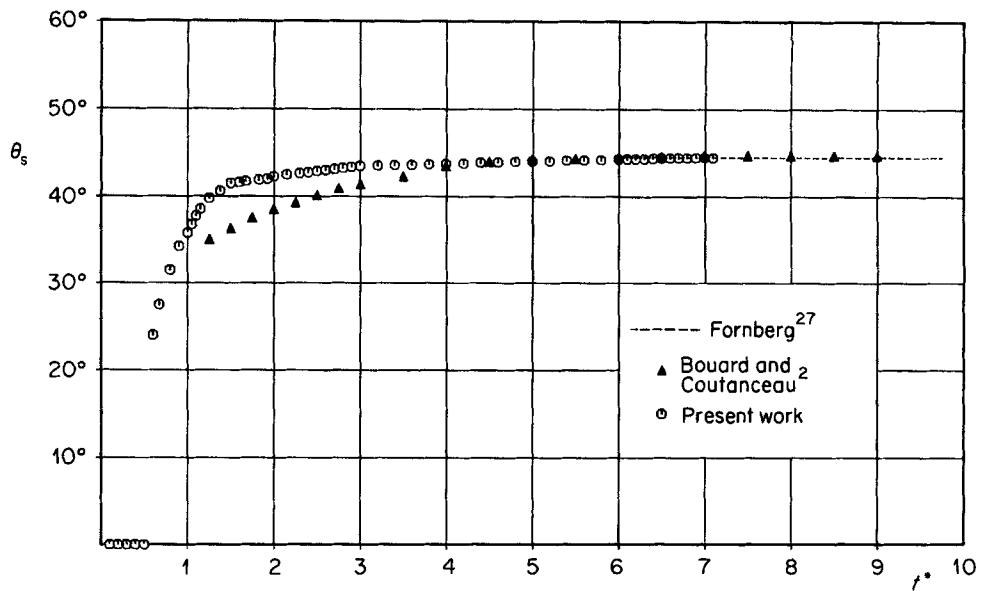


Figure 6. Evolution of the separation angle θ_s according to Bouard and Coutanceau,⁴ to Fornberg²⁷ and to the present work

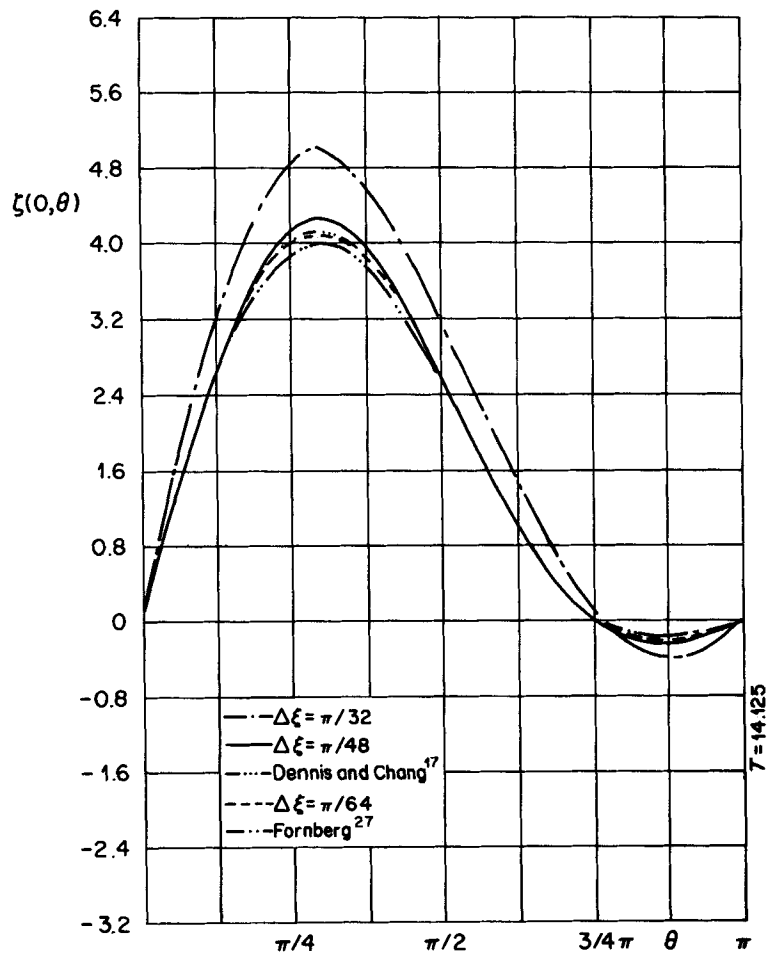


Figure 7. A comparison among steady-state calculations for the vorticity at the cylinder's surface ($Re = 20$)

is good in comparison with the experimental results mentioned earlier.

Steady state asymptotic solutions have been plotted as well. They range from $L/D = 0.90$ to approximately $L/D = 0.10$.

Figure 6 shows the development of the separation angle θ_s (corresponding to the separation of the main flow from the wall of the cylinder) for $\Delta\xi = \pi/64$ (and a choice of method 5 for the boundary condition). The early development of θ_s does not match the experimental results of Coutanceau and Bouard but the laboratory measurements are not very trustworthy during the initial stage of the flow (quoting the authors) due to very small values and abrupt growth of the wake at $t = 0.5$ so that cumulative errors are reported to result in length and time measurements. In the present calculations the angle θ_s is measured at the null value of wall vorticity. Later the calculated separation angle matches the measured θ_s curve (the asymptotic value $\theta_s = 44.98^\circ$ matches, in fact, both experimental and numerical results).

Further comparisons

Figure 7 shows a comparison of the steady-state wall vorticity distribution with the numerical results of Dennis and Chang¹⁷ and Fornberg.²⁷ The agreement with the present results for $\Delta\xi = \pi/64$ is considered satisfactory. Figure 7 also presents the wall vorticity distributions at $t = 14.25$ for the present simulations using $\Delta\xi = \pi/16$ and $\Delta\xi = \pi/32$. The overestimation of vorticity at larger mesh sizes is manifest.

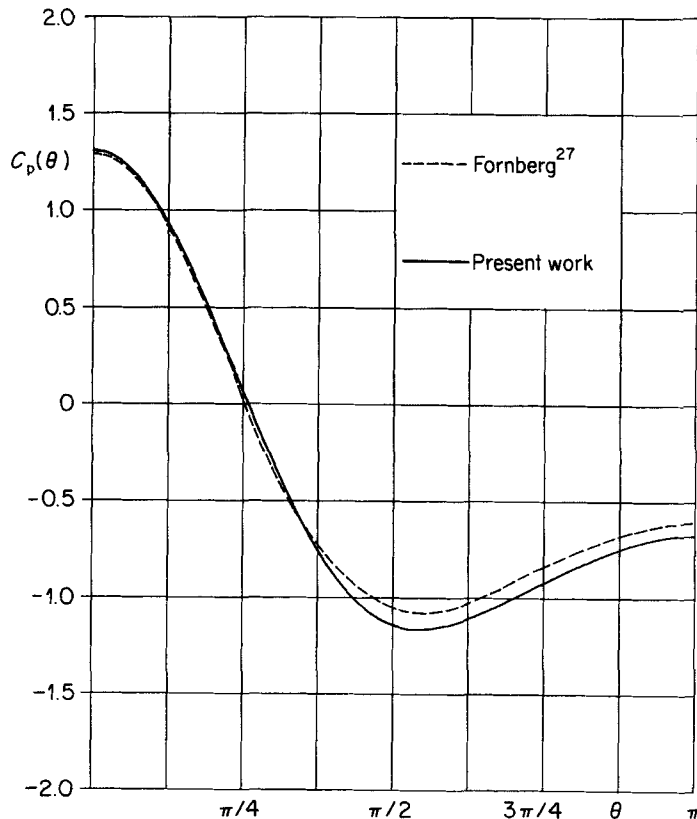


Figure 8. A comparison between steady-state pressure coefficient distribution at the cylinder's surface ($Re = 20$)

Figure 8 shows the steady state pressure coefficient at the body's surface, as compared with Fornberg's calculations. The calculated results for the front stagnation pressure coefficient C_{ps} ($C_{ps} = 1.29$ for $\Delta\xi = \pi/64$) respect also the limit law which rules the viscous overpressure at the stagnation point.³² An excess of vorticity in the back of the cylinder (apparently responsible also for longer wakes for $\Delta\xi > \pi/64$) creates an excess of negative pressures in the rear zone, noticeably reduced at $\Delta\xi = \pi/64$. The overall agreement is nevertheless deemed satisfactory.

The calculated total drag coefficients are presented in Table I for the coarser and the 'optimal' mesh size. The calculated drag coefficients are compared with analogous values found in the literature for the case study at $Re = 20$.

CONCLUSIONS

The paper deals with development and calibration of an algorithm for the calculation of unsteady viscous fluid flow about an impulsively started cylinder.

The algorithm consists of a discrete Fourier transform expansion of the flow fields. The procedure makes use of fast numerical methods for the evaluation of non-linear convolution sums which portray the convective terms of the Navier-Stokes equations in Fourier space. The two coupled second-order parabolic and elliptic differential equations for Fourier coefficients have been solved by finite difference techniques.

Suitable boundary condition schemes at the outer field and at the solid wall have been studied in order to point out a seemingly optimal choice for the numerical simulations.

The numerical approach, which has been designed to overcome certain numerical difficulties for high Reynolds number simulations, has been tested via the calculation of the flow past an impulsively started cylinder at $Re = 20$. This regime has, in fact, received much attention, hence yielding an ideal test case for all scalar and vectorial fields.

Time development of the symmetrical standing zone of recirculation, which is formed in the early stage of the flow, has been studied for $300 \leq Re \leq 9500$. Even though optimal choices for $Re = 20$

Table I. Comparison among values of the drag coefficients at $Re = 20$

Author	Comments	Drag coefficients
Thom ³	Arithmetical solution (hand calculation)	2.180
Dennis and Chang ¹⁷	Numerical solution (time dependent calculations)	2.045
Takami and Keller ¹⁵	Numerical solution (time dependent calculations)	2.003
Tritton ⁴²	Experimental measurements	2.100
Nieuwstadt and Keller ¹⁹	Numerical solution (steady state calculations)	2.053
Fornberg ²⁷	Numerical solution (steady state calculations)	2.010
Present work	$\zeta_{\kappa}(0, t)$ as in Method 5 ($\Delta\xi = \pi/64$)	2.092
Present work	$\zeta_{\kappa}(0, t)$ as in Method 5 ($\Delta\xi = \pi/32$)	2.331
Present work	$\zeta_{\kappa}(0, t)$ as in Method 5 ($\Delta\xi = \pi/16$)	2.783

may not be optimal for Re as high as 9500, comparison of computed results with experimental visualizations has been favourable.³⁶ Results of the simulation and discussion will be presented in a companion paper.

REFERENCES

1. P. J. Roache, *Computational Fluid Dynamics*, Hermosa, Albuquerque, 1976.
2. R. Bouard and M. Coutanceau, 'The early stage of development of the wake behind an impulsively started cylinder for $40 < Re < 10^4$ ', *Journal of Fluid Mechanics*, **101**, (3), (1980).
3. A. Thom, 'The flow past circular cylinders at low speeds', *Proceedings of the Royal Society, London, A*, **9**, (1933).
4. M. Kawaguti, 'Numerical solution of the Navier–Stokes equations for the flow around a circular cylinder at Reynolds number 40', *Journal of the Physical Society of Japan*, **8**, (1953).
5. G. Allen and R. V. Southwell, 'Relaxation methods applied to determine the motion in two dimensions of a viscous fluid past a fixed cylinder', *Quarterly Journal of Mechanics and Applied Mathematics*, **VIII**, (2), (1955).
6. R. B. Payne, 'Calculations of unsteady viscous flow past a circular cylinder', *Journal of Fluid Mechanics*, **4**, (1958).
7. P. C. Jain and M. Kawaguti, 'Numerical study of a viscous fluid past a circular cylinder', *Journal of the Physical Society of Japan*, **21**, (1966).
8. H. B. Keller and H. Takami, 'Numerical studies of viscous flow about cylinders', in D. Greenspan (ed.), *Numerical Solutions of Nonlinear Differential Equations*, Wiley, London, 1966.
9. D. B. Ingham, 'Note on the numerical solution for unsteady viscous flow past a circular cylinder', *Journal of Fluid Mechanics*, **31**, (4), (1968).
10. C. J. Apelt, 'The steady flow of a viscous fluid past a circular cylinder at Reynolds numbers 40 and 44', Aeronautical Research Council, London, *Reports & Memoranda, No. 3175* (1958).
11. A. E. Hamielec and J. D. Raal, 'Numerical studies of viscous flow around circular cylinders', *The Physics of Fluids*, **12**, (1), (1969).
12. P. C. Jain and K. Sankara Rao, 'Numerical solution of unsteady viscous incompressible fluid flow past a circular cylinder', *Physics of Fluids Supplements*, **II**, (1969).
13. J. S. Son and T. J. Hanratty, 'Numerical solution for the flow around a cylinder at Reynolds numbers of 40, 200 and 500', *Journal of Fluid Mechanics*, **92**, (1979).
14. D. C. Thoman and A. A. Szewczyk, 'Time dependent viscous flow over a circular cylinder', *Physics of Fluids Supplement*, **II**, (1969).
15. H. Takami and H. B. Keller, 'Steady two-dimensional viscous flow of an incompressible fluid past a circular cylinder', *Physics of Fluids Supplements*, **II**, (1969).
16. R. L. Underwood, 'Calculations of incompressible flow past a circular cylinder at moderate Reynolds numbers', *Journal of Fluid Mechanics*, **37**, (1969).
17. S. C. R. Dennis and Gau Zu Chang, 'Numerical solutions for steady flow past a circular cylinder at Reynolds numbers up to 100', *Journal of Fluid Mechanics*, **42**, (3), (1970).
18. J. C. Wu and J. F. Thompson, 'Numerical solutions of time-dependent incompressible Navier–Stokes equations using an integro-differential formulation', *Computers and Fluids*, **1**, (1973).
19. F. Nieuwstadt and H. B. Keller, 'Viscous flow past circular cylinders', *Computers and Fluids*, **1**, (1973).
20. W. M. Collins and S. C. R. Dennis, 'Flow past an impulsively started circular cylinder', *Journal of Fluid Mechanics*, **60**, (1), (1973).
21. V. A. Guschin and V. V. Schennikov, 'A numerical method of solving the Navier–Stokes equations, *Za. Vychist. Mat. Mat. Fiz.*, **14**, (1974).
22. P. K. G. Panikker and Z. Lavan, 'Flow past impulsively started bodies using Green's function', *Journal of Computational Physics*, **18**, (1975).
23. P. L. Ta, 'Etude numerique de l'ecoulement d'un fluide visqueux incompressible autour d'un cylindre fixe en rotation. Effect Magnus', *Journal du Mecanique*, **14**, (1975).
24. V. A. Patel, 'Time-dependent solutions of the viscous incompressible flow past a circular cylinder by the method of series truncation', *Computers and Fluids*, **4**, (1976).
25. C. L. Lin, D. W. Pepper and S. C. Lee, 'Numerical methods for separated flow solutions around a circular cylinder', *AIAA Journal*, **14**, (1), (1976).
26. S. Y. Tuann and M. D. Olson, 'Numerical studies of the flow around a circular cylinder by a finite element method', *Computer and Fluids*, **6**, (1978).
27. B. Fornberg, 'A numerical study of steady viscous flow past a circular cylinder', *Journal of Fluid Mechanics*, **98**, (4), (1980).
28. P. L. Ta, 'Numerical analysis of unsteady secondary vortices generated by an impulsively started circular cylinder', *Journal of Fluid Mechanics*, **100**, (1), (1980).
29. A. Giorgini and J. R. Travis, 'A short convection', Tech. Rep. no. 26, Water Resources and Hydromechanics Laboratory, School of Civil Engineering, Purdue University, West Lafayette, Indiana 47907, (1969).
30. W. M. Collins and S. C. R. Dennis, 'The initial flow past an impulsively started circular cylinder', *Quart. Journal of Mechanics and Applied Mathematics*, **26**, (1), (1973).

31. J. W. Cooley and J. W. Tukey, 'An algorithm for the machine calculation of complex Fourier series', *Mathematics of Computation*, **19**, (1965).
32. Aldo Giorgini and A. Rinaldo, 'A mixed discrete Fourier transform-quasi analytical algorithm for the solution of the Navier-Stokes equations', Proceedings of International Symposium on Refined Modelling of Flow, IAHR, Paris, (France). Vol. 1, 1982.
33. A. Thom, 'Arithmetical solution of problems in steady viscous flow', Aeronautical Research Committee, *Reports and Memoranda*, No. 1475 (1932).
34. Jensen, (1959), (Reported in Roache¹).
35. Briley, (1970), (Reported in Roache¹).
36. A. Rinaldo, 'A mixed discrete Fourier transform-finite difference algorithm for the solution of the Navier-Stokes equations', *Ph.D. Dissertation*, Purdue University, West Lafayette, Indiana, May 1983.
37. I. Imai, 'On the asymptotic behaviour of viscous fluid flow at a great distance from a cylindrical body, with special reference to Filon's paradox', *Proceedings of the Royal Society, London*, **12**, (1951).
38. A. Giorgini 'Far field boundary conditions in computational fluid mechanics', *Technical Report CE-HSE-83-8*, School of Civil Engineering, Purdue University, West Lafayette, Indiana, 1983.
39. Woods, (1954). (Reported in Roache¹).
40. R. Bouard and M. Coutanceau, 'Experimental determination of the main features of the viscous flow in the wake of a circular cylinder in uniform translation. Part 1. Steady flow', *Journal of Fluid Mechanics*, **79**, (2), (1977).
41. M. Coutanceau and R. Bouard, 'Experimental determination of the main features of the viscous flow in the wake of a circular cylinder in uniform translation. Part 2. Unsteady Flow', *Journal of Fluid Mechanics*, **79**, (2), (1977).
42. D. J. Tritton, 'Experiments on the flow past a circular cylinder at low Reynolds numbers', *Journal of Fluid Mechanics*, **16**, (4), (1959).
43. J. W. Cooley, P. A. Lewis and P. D. Welch, 'The fast Fourier transform algorithm: programming considerations in the calculation of sine, cosine and Laplace transforms', *Journal of Sound Vibration*, **13**, (3), (1970).
44. S. A. Orszag, 'Transform method for the calculation of vector-coupled sums: application to the spectral form of the vorticity equation', *Journal of the Atmospheric Sciences*, **12**, (1970).
45. S. A. Orszag, 'Numerical simulation of incompressible flows within simple boundaries: accuracy', *Journal of Fluid Mechanics*, **49**, (1), (1971).
46. A. Rinaldo and Aldo Giorgini, 'Discrete Fourier transform-quasi analytical algorithm for the solution of the Navier-Stokes equations: error analysis', *Technical Report CE-HSE-82-18*, Hydraulic and Systems Engineering, School of Civil Engineering, Purdue University, West Lafayette, Indiana, 1982.